NUMERICAL SIMULATION OF OXYGEN-ENRICHED COMBUSTION IN A PRECALCINER USING COAL GANGUE-BLENDED PULVERIZED FUEL

Jie WANG[a], Long CHEN[a], and Hongtao KAO[a]*

[a] College of Materials Science and Engineering, Nanjing Tech University, Nanjing 211816, China

*Corresponding author: Prof. Hongtao Kao, E-mail: kaoht@163.com

Abstract: *This study emphasizes the potential role of coal gangue as an alternative fuel and oxygen-enriched combustion technology within TTF precalciners(Twin-Tank Furnace) in mitigating carbon emissions from cement production. The research primarily unfolds in two segments. Initially, the investigation addresses the influence of blending varying proportions of coal gangue under an air atmosphere on the internal temperature field and raw material decomposition components within the precalciner, aiming to discern the optimal blending ratio. Subsequently, the study simulates combustion under different oxygen-enriched atmospheres at the ideal coal-gangue blending ratio, establishing the combustion patterns under these conditions. Although the mixed fuel prompts symmetry in the flow field and temperature field, the distinct combustion characteristics of coal gangue and coal powder—following a 20% coal gangue blend—lead to an accelerated mainstream velocity and abbreviated fuel residence time. Consequently, the exit temperature and CO_2 concentration diminish with increasing blending content, reaching an optimal raw material decomposition rate of 91.12% within the precalciner when blended with 20% coal gangue. Furthermore, in oxygen-enriched combustion, as the oxygen content escalates, both the average temperature at the precalciner's exit and the raw material decomposition rate witness an upsurge, whereas the average CO_2 concentration at the outlet experiences a decline.*

Keywords: *Numerical Simulation; Precalciner Combustion; Coal Gangue Alternative Fuel; Oxygen-enriched Combustion.*

1. Introduction

Cement, a crucial raw material for national infrastructure development, is at the crossroads of considerable challenges such as high energy consumption, substantial emissions, and overcapacity. Studies have explored the principles and current status of low-carbon production methods in the cement industry, summarizing emission reduction technologies such as alternative raw materials, fuel substitution, and clinker substitution based on existing CO_2 emission reduction technologies [1]. This paper primarily focuses on the simulation study combining partial alternative fuels and oxygen-enriched combustion technology. Utilizing coal gangue as a substitute for coal combustion in

cement production not only conserves coal resources but also results in lower pollution, representing a new type of environmentally friendly and efficient method of coal gangue resource utilization. Additionally, coal gangue contains components like SiO_2 and CaO that are suitable for cement production raw materials, thereby reducing the consumption of resources such as clay and limestone [2]. Consequently, coal gangue's application as an alternative fuel holds broad prospects in cement production. Due to its low calorific value, coal gangue's combustion characteristics can be studied in comparison with inferior coal powder[3]. Currently, research on coal gangue combustion characteristics mainly focuses on two aspects: first, exploring coal gangue's combustion properties and material transformation rules during combustion through thermal analysis and blended combustion tests [4]; second, investigating the applicability, combustion efficiency, and combustion products of coal gangue combustion technology, including fluidized bed combustion, rotary kiln combustion, and fixed-bed combustion. Zhang et al. [5] studied the combustion characteristics of coal gangue with different ash contents through thermogravimetric experiments, indicating that the overall combustion efficiency and comprehensive combustibility index of coal gangue significantly increase with a reduction in ash content. Xiao et al. [6] conducted experimental research on the co-combustion characteristics of coal gangue, sludge, and coal powder, finding that adding coal powder to coal gangue and sludge fuel significantly enhances combustion efficiency. Li et al. [7] examined coal gangue's combustion behavior and kinetic models under different heating rates in an air atmosphere through experiments. Zhou et al. [8] discovered through thermogravimetric experiments that doping biomass in coal gangue could improve its ignition properties and thermal reaction characteristics, determining the optimal doping ratio.

Using oxygen-rich combustion in the precalciner is a common low-carbon production method that has many benefits, such as raising the precalciner's internal temperature, lowering the fuel's ignition points, speeding up combustion rates, improving combustion completion, lowering dust pollution, boosting combustion effects, raising clinker quality, and raising production yields. Due to the high internal temperatures and dust concentrations within the precalciner, experimental research is challenging. However, numerical simulation enables the prediction and optimization of various production parameters and processes prior to actual production. This approach helps diminish the necessity for trials and errors, thereby saving time and costs. Consequently, numerical simulation constitutes an effective methodology for researching the oxygen-enriched combustion process of coal gangue in precalciners. Fu et al. [9] conducted oxygen-enriched air gasification experiments in a fluidized bed gasifier to analyze factors affecting the gasification characteristics of Refuse Derived Fuel, discovering that the volumetric fraction of combustible components rapidly increases with enhanced oxygen content, significantly improving gasification efficiency under oxygen-enriched conditions. Zhang et al. [10] utilized numerical simulation techniques to comparatively study the generation of NO within TTF precalciners under different atmospheres, noting that the NO emission concentration at the precalciner outlet under the O_2/CO_2 atmosphere was significantly reduced compared to other atmospheres. Fidaros et al [11] introduced a numerical model for flow and transport processes inside the precalciner, applying the k-ε model to simulate the impact of turbulence, achieving data on fluid velocity, temperature and concentration distribution of substances, particle trajectories within the furnace, and gas-solid coupling processes. Wang et al. [12] explored the combustion thermodynamic characteristics and pollutant emissions of diesel in various oxygen-enriched atmospheres through numerical simulation, indicating that an oxygen-rich

atmosphere enhances combustion temperature, flame temperature gradient, combustion heat release rate, and flame propagation velocity.

From the aforementioned studies, it can be concluded that the combustion technology of coal gangue as an alternative fuel in cement production still requires further refinement. Oxygen-enriched combustion can further optimize and improve coal-gangue substitute fuel combustion technology. However, current research on oxygen-enriched combustion in precalciners under coal powder and coal gangue mixed fuel conditions is relatively insufficient, particularly concerning gas flow and heat transfer characteristics during the combustion process. This deficiency necessitates further strengthening. Additionally, when the coal gangue blending ratio is excessively high, issues related to combustion, heat transfer, and desulfurization within the precalciner may arise due to the low calorific value, increased ash content, and high sulfur content. This research is premised on selecting the optimal blending ratio under different coal gangue and coal powder fuel combustion conditions and analyzing the combustion circumstances within the precalciner under various oxygen-enriched atmospheres at the optimal coal gangue and coal powder fuel ratio.

To simulate the process of coal dust combustion and raw material decomposition in a TTF precalciner, it is very important to use the popular Computational Fluid Dynamics (CFD) software Fluent [13]. This study targets an actual decomposing furnace in a cement plant, employing Fluent for the numerical simulation of oxygen-rich combustion in the furnace based on pulverized coal mixed with coal gangue fuel. The research yields distributions of temperature fields and component concentration fields. The results not only furnish practical operational references for combustion within this precalciner but also provide a basis for further improvement of coal dust and coal gangue combustion technology in such precalciners.

2. Mathematical Model and Numerical Methods

The fluid within the decomposing furnace inevitably adheres to the laws of mass, momentum, and energy conservation during flow. This paper adopts an eddy dissipation model for simulating coal dust combustion and employs the P1 radiation model for handling radiative heat transfer [14, 15]. The Discrete Phase Model (DPM) is utilized to simulate the motion of solid-phase particles in the gaseous phase [16, 17].

2.1. Basic control equations

Basic physical conservation laws govern fluid flow, including the laws of conservation of mass, momentum and energy. The mathematical description of these laws is known as governing equations.

(1) The mass conservation equation, where the increase in mass per unit time in a fluid calculation cell is equal to the net mass flowing into that cell during the same time step, is given by the following formula:

$$\frac{\partial \rho}{\partial t} + \nabla \cdot (\rho \vec{u}) = 0 \#(1)$$

Where,ρ represents the density; t represents the time; $\vec{u}$ represents the velocity vector.

(2) Conservation of momentum equation, the rate of change of the momentum of the fluid in the calculation cell in time is equal to the sum of the external forces used in the calculation cell , the formula is as follows:

$$\frac{\partial(\rho u)}{\partial t} + \mathrm{div}(\rho u\vec{u}) = -\frac{\partial p}{\partial x} + \mathrm{div}(\mu \mathrm{grad} u) + S_u \#(2)$$

$$\frac{\partial(\rho v)}{\partial t} + \mathrm{div}(\rho v\vec{u}) = -\frac{\partial p}{\partial y} + \mathrm{div}(\mu \mathrm{grad} v) + S_v \#(3)$$

$$\frac{\partial(\rho w)}{\partial t} + \mathrm{div}(\rho w\vec{u}) = -\frac{\partial p}{\partial z} + \mathrm{div}(\mu \mathrm{grad} w) + S_w \#(4)$$

ρ represents the density; p represents the static pressure; μ represents the hydrodynamic viscosity; S represents the generalised source term of the conservation equation; $\vec{u}$ represents the velocity.

(3) The energy conservation equation, the rate of increase of energy in the calculation cell is equal to the net heat flow into the calculation cell plus the work done by the forces applied to the surface and volume elements of the calculation cell, is given by the following formula:

$$\frac{\partial(\rho h)}{\partial t} + \frac{\partial(\rho \mu_i h)}{\partial x_i} = -p\mathrm{div}\vec{u} + \mathrm{div}(\lambda \mathrm{grad} T) + \phi + S_h \#(5)$$

where: h represents the fluid ratio; λ represents the thermal conductivity of the fluid; S_h represents the internal heat source; ϕ represents the dissipation function equation of state.

2.2. Gaseous Phase Turbulence Model

Given the substantial mass flow of flue gas and tertiary air entering the decomposing furnace, yet with relatively small inlet cross-sectional areas, there is a need to comprehensively consider employing the more widely applicable Realizable k-ε model to simulate gaseous phase turbulent flow within the furnace [18]. The transport equations for turbulent kinetic energy and dissipation used in this model are as follows:

$$\frac{\partial}{\partial x_j}(\rho k u_j) + \frac{\partial}{\partial t}(\rho k) = \frac{\partial}{\partial x_j}\left[\left(\frac{u_t}{\sigma_k} + u\right)\frac{\partial k}{\partial x_j}\right] - \rho\varepsilon - Y_M + G_k + G_b + S_k \#(6)$$

$$\frac{\partial}{\partial x_j}(\rho \varepsilon u_j) + \frac{\partial}{\partial t}(\rho \varepsilon) = \frac{\partial}{\partial x_j}\left[\left(\frac{u_t}{\sigma_\varepsilon} + u\right)\frac{\partial \varepsilon}{\partial x_j}\right] - 1.9\rho\frac{\varepsilon^2}{k + \sqrt{v\varepsilon}} - 1.44\frac{\varepsilon}{k}C_{3\varepsilon}G_b + \rho C_1 S\varepsilon + S_\varepsilon \#(7)$$

$$C_1 = max\left[0.43\frac{\eta}{\eta + 5}\right], \eta = S\frac{k}{\varepsilon} \#(8)$$

Where, G_b represents the production of turbulent kinetic energy due to buoyancy; G_k represents the production of turbulent kinetic energy due to the velocity gradients; Y_M represents the contribution of turbulent dilation to the dissipation rate; σ_ε and σ_k represent the turbulent Prandtl numbers for the ε and k; S_ε and S_k represent custom source terms.

2.3. Raw Material Decomposition Model

In researching the decomposition reactions of raw materials in the furnace, domestic scholars primarily focus on $CaCO_3$ decomposition. To simplify the mathematical model, raw materials are approximated as $CaCO_3$. The decomposition of $CaCO_3$ involves thermodynamic and kinetic processes [19]. The reaction process of $CaCO_3$ decomposition is as follows:

$$CaCO_3(s) \xrightarrow{\Delta H = +\frac{171KJ}{mol}} CaO(s) + CO_2(g) \#(9)$$

The decomposition rate equation for raw materials can be expressed as:

$$\frac{dx}{dt} = k(1-x) * e^{-\frac{E}{RT}} \#(10)$$

Where, k represents the decomposition reaction rate constant; x represents the fraction of undecomposed raw materials; E represents the activation energy; R represents the universal gas constant; T represents the reaction temperature. The activation energy for the decomposition of calcium carbonate is 171 kJ/mol, and the pre-exponential factor is $1\times10^{7}s^{-1}$.The decomposition rate of raw materials is generally defined as:

$$\eta = \frac{m_1 - m_2}{m_1} \times 100\% \#(11)$$

Among them, m_1 represents the mass flow rate of $CaCO_3$ at the entrance, and m_2 represents the mass flow rate of $CaCO_3$ at the outlet.

2.4. Fuel Combustion Model

Cement precalciners typically utilize pulverized coal as fuel, and this study additionally involves coal gangue. Inorganic oxides in coal gangue can be included in raw material components, considering coal gangue as an inferior pulverized coal fuel. The combustion of pulverized coal injected into the precalciner first involves the release and combustion of volatiles, followed by the combustion of residual coal particles. The pyrolysis process of coal powder adopts the two-step competitive rate model proposed by Kobayashi [20]. The release rate of volatiles is expressed as follows:

$$\frac{m_v(t)}{m_{p,0} - m_a} = \int_0^t (a_1 R_1 + a_2 R_2) \exp\left(- \int_0^t (R_1 + R_2)\, dt \right) dt \#(12)$$

$m_v(t)$ represents the mass of volatile matter released from pulverized coal during the reaction time; $m_{p,0}$-m_a represents the dry ash free mass of the particle; R_1 and R_2 represent the reaction rate constants obtained through the Arrhenius equation; a_1 and a_2 represent the low-temperature release rate factor and the high-temperature volatile release rate factor, respectively.

After the release and combustion of volatiles, the remaining coal initiates surface combustion reactions. The Fluent software involves several coal particle chemical reaction models, including the diffusion reaction model, kinetic/diffusion-controlled reaction model, internal control reaction rate model, and multi-step surface reaction model. The coal combustion rate is [21]:

$$\frac{dm_p}{dt} = -\pi d_p^2 P_{ox} \frac{k_1 k_2}{k_1 + k_2} \#(13)$$

d_p represents the granule diameter; P_{ox} represents the partial pressure of oxygen around the coal particles; k_1 represents the diffusion factor of oxygen to the coal particle surface; k_2 represents the reaction kinetics coefficient.

2.5. Radiative heat transfer model

In the precalciner, there are many kinds of heat exchange modes, and in these complex heat exchange processes, the radiation heat exchange accounts for more than 95% of the total heat exchange in the furnace, so the radiation heat exchange model is mainly used to calculate the heat exchange process in the precalciner in the simulation calculation. Because of the existence of radiative heat exchange between gas and solid in the precalciner, the P1 radiation model is chosen in this study. The heat transfer equation for P1 radiation is as follows:

$$\frac{Q_e}{Q}+\frac{Q_d}{Q}+\frac{Q_r}{Q}=1\#(14)\#$$

$$q_r=\frac{d_Q}{dt}=-\frac{1}{(3(a+\sigma_s)-C\sigma_s)}\nabla G\#(15)$$

The transport equation for the incident radiation G:

$$\nabla\cdot(\Gamma\nabla G)-aG+4an^2\sigma T^4=S_G\#(16)$$

$$-\nabla\cdot q_r=aG-4an^2\sigma T^4\#(17)$$

Q_e / Q represents the absorptivity; Q_d / Q represents the transmittance; Q_r / Q represents the reflectance; q_r represents the radiant flux; a represents the absorption; σ_s represents the scattering coefficient; G represents the incident radiation; C represents the linear anisotropic phase function coefficient; n represents the refractive index of the medium; σ represents the Stefan-Boltzmann constant; S_G represents the user-defined radiation source.

3. Geometric Model and Boundary Conditions

3.1. Geometric Model

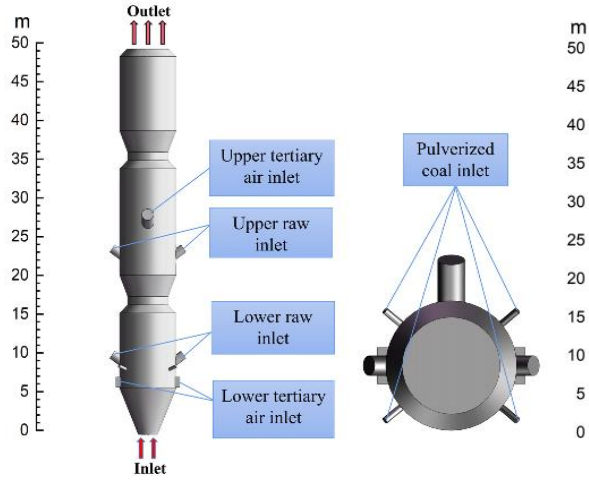

Fig.1 Calculation domain model of precalciner

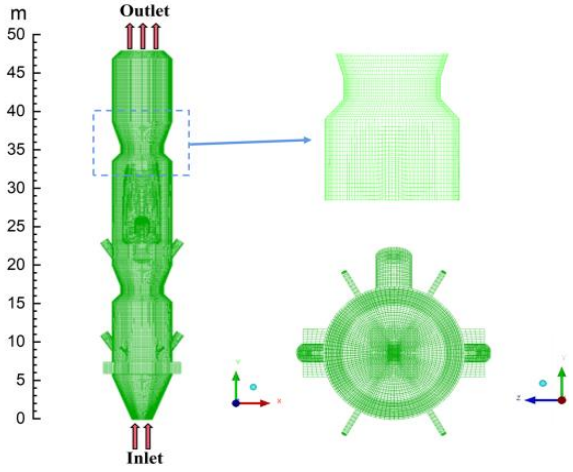

Fig. 2 Global mesh and local enlargement of the precalciner

As depicted in Fig 1, the total height of the furnace body is 48.3 meters, divided into three sections. The bottom section, designated for high-temperature flue gas entry, has a diameter of 1.85 meters, while the top, serving as the precalciner exit, measures 2.5 meters in diameter. The furnace body incorporates three tertiary air ducts, with two located in the lower column and one in the middle column. Both the bottom and middle columns are equipped with two feed pipes each, and four coal injection pipes are situated 0.7 meters above the lower tertiary air inlet.

After the model is established, it needs to be divided into meshes for calculation, and ICEM software is chosen to divide the meshes in this study. The decomposition furnace is divided into a hexahedral structured mesh after comprehensively considering the characteristics of the calculation

object, calculation accuracy requirements and calculation resources. Fig 2 illustrates the grid diagram of the precalciner.

3.2. Grid Validation

To ensure the accuracy of computational results, grid independence requires verification. This study selected five different grid counts: 325,680; 662,436; 885,642; 1,002,566; and 1,225,658, examining the temperature fields under these grid counts in coal dust conditions. Points were chosen every 5 meters along the positive direction of the calciner's Z-axis, totaling ten, to compare their temperature values. As shown in Fig 3, the temperature variation curves in the calciner under the latter three grid counts are essentially consistent, indicating that the computational results under these grid numbers have stabilized, achieving grid independence. Therefore, considering both computational accuracy and speed, this study opts for a grid count of 885,642 for subsequent simulations.

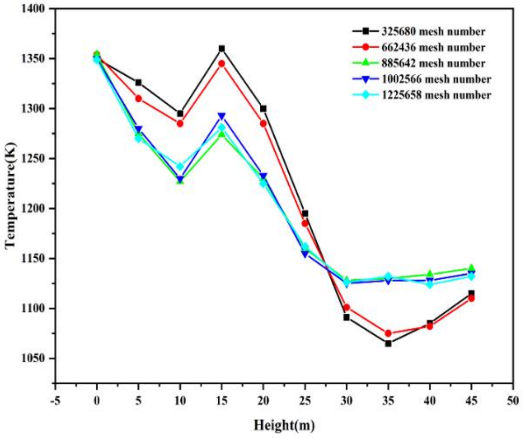

Fig. 3 Precalciner temperature versus grid number

3.3. Boundary Conditions

The boundary conditions employed in this study are derived from actual data collected through thermal calibration at a cement plant. Both the kiln tail flue gas inlet and the tertiary air inlet adopt a uniform velocity distribution, with the flue gas speed being 27 m/s and its temperature 1350 K. The boundary condition for the precalciner outlet is a pressure outlet, with the outlet pressure being -500 Pa. The particle phase at the outlet is set for escape, while other inlet boundaries are set for reflection. The precalciner adopts a no-slip boundary condition for the wall, with the fluid near the wall using standard wall functions. Boundary parameters for tertiary air inlets, coal powder inlet and raw material inlet are shown in Tab 1. The air excess factor in the simulation is 1.1. The coal powder inlet and raw material inlet utilize a mass flow inlet as the boundary condition. The particle size distribution of gangue is the same as that of coal dust.The particle sizes of pulverized coal and raw material were calculated by Rosin-Rammler distribution function. The maximum particle size of pulverized coal was 80 μm the minimum particle size was 20 μm, and the average particle size was 60 μm. The maximum particle size of raw material was 50 μm; the minimum particle size was 30 μm, and the average particle size was 40 μm. The component analysis of the raw materials is presented in Tab 2. Industrial and chemical analyses of coal powder and coal gangue are as depicted in Tab 3.

Table 1. Boundary parameters for tertiary air inlets, coal powder inlet and raw material inlet

Parameter	Coal	Tertiary air inlet		Raw material	
		Lower	Upper	Lower	Upper
Pressure value(Pa)	-550	-520	-1200	-720	-1000
Velocity Inlet（m/s）	/	26	26	/	/
Mass flow (kg/s)	1.25	/	/	15.3	21.2
Temperature (K)	337	1250	1250	1045	1045

Table 2.Raw material compositions/wt%

SiO_2	Al_2O_3	Fe_2O_3	CaO	MgO	Loss on ignition(LOI)
12.17	3.74	2.63	43.96	0.17	35.37

Table 3.Proximate analysis and elemental analysis of the data of coal and coal gangue

Sample	Proximate analysis（%）				Ultimate analysis（%）					$Q_{net,ar}$
	M_{ad}	A_{ad}	V_{ad}	FC_{ad}	C_{ad}	H_{ad}	O_{ad}	N_{ad}	S_{ad}	(MJ/Kg)
Coal	1.78	24.89	22.30	51.03	64.21	3.79	27.64	3.06	1.3	24.81
Coal gangue	1.61	35.44	14.58	48.37	59.33	5.93	29.37	3.61	1.76	11.773

This study is primarily divided into two parts. In the first part, in order to reveal the transport law of gas-solid two-phase flow in the precalciner after partial replacement of pulverised coal with 0%, 10%, 20%, 30% and 40% of gangue by mass mixing ratios in an air ambient (with an oxygen content of 21%), the temperature fields of the various constituents in the chamber, the decomposition of the raw materials as well as the constituents of the separated coals under combustion were compared and analysed to determine the optimal coal ratios. Translated with www.DeepL.com/Translator (free version) In the second part, while ensuring the total heat entering the furnace remains constant, combustion under four different oxygen-enriched atmospheres at the optimal blending ratio was simulated. The respective oxygen concentration proportions were 25%, 30%, 35%, and 40%. By comparing and analyzing the simulation results, the study sought to identify the optimal oxygen-rich atmosphere where raw material combustion characteristics and decomposition rate are minimally affected, thereby achieving the highest decomposition rate under normal precalciner operation conditions.

4. Simulation Results and Analysis

4.1. Combustion simulation at Different Gangue Blending Ratios

4.1.1 Validation of Numerical Simulation Results

Table 4.Comparisons between the simulation and measurements

Parameter	Pulverized coal combustion prediction value	Measured value	Error
Outlet temperature	1194K	1177K	1.7%
Raw material decomposition rate	92.99%	92.35%	1.4%
CO_2 mole fraction	22.51%	21.69%	3.6%

To verify the reliability of the simulation outcomes, this research juxtaposed the measured data with the primary parameters at the precalciner outlet post-simulation. As indicated in Tab 4, the relative errors of the precalciner outlet temperature, carbon dioxide content, and raw material decomposition rate under pure coal combustion conditions are all within 4%, falling within the permissible engineering range. This demonstrates the reliability of the data obtained from numerical simulations. The results not only offer theoretical guidance for the actual operation of precalciners but also lay the groundwork for subsequent studies on the impact of oxygen-enriched combustion of coal-gangue blended fuels within such precalciners.

4.1.2 Comparative Analysis of Temperature Distribution

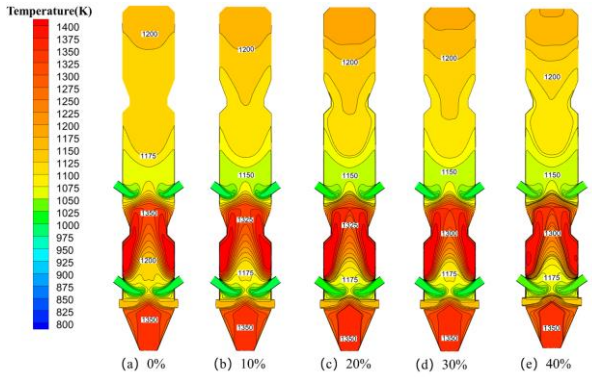

Fig. 4 Temperature distribution under different gangue mixing ratio

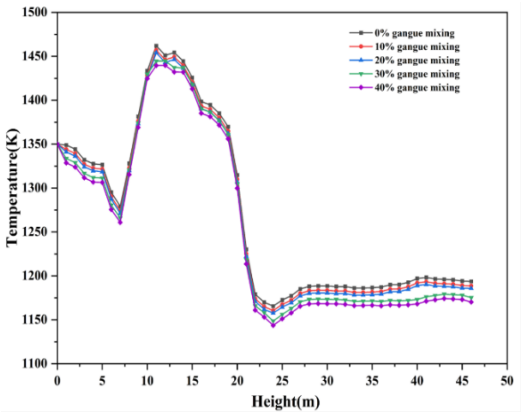

Fig. 5 Average temperature under different different gangue mixing ratio

Fig 4 illustrates the isothermal contour maps of the X-sectional (Positional cross-section of the precalciner on the X-axis) temperature field distribution under five different operational scenarios. It is observed that the temperature field distributions in the blending scenarios are akin to those in the single fuel scenarios, displaying symmetry about the X-section, indicating that the fuels are fully combusted under different blended conditions. High-temperature zones predominantly localize alongside the cone, the upper coal burner, and the tertiary air duct areas. A minimal amount of fuel, due to the retention effect of the material dispersing box, drifts to the opposite side, forming elongated high-temperature bands on both sides. This area expands as the fuel quantity increases. The

low-temperature zones are primarily around the upper and lower raw material inlets. With the increase of gangue content, the maximum temperature of the high temperature zone decreases from 1350 K to 1300 K. And when the gangue content is more than 20%, the temperature at the initial position of the high temperature zone starts to decrease. As depicted in Fig5, there are two temperature peaks, attributable to the exothermic reactions of the fuel at the lower and upper levels, respectively. Given the identical heights of the upper burner and the material dispersing box, a significant temperature drop is noted within the furnace segment, spanning 13m to 20m in height, due to the substantial heat absorption by raw materials. From approximately 24m to 29m, the injection of upper tertiary air leads to continued combustion of unburnt materials and the decomposition of raw materials, first elevating the temperature, followed by a subsequent decline. Ultimately, the average outlet temperature values for coal gangue blending ratios of 0%, 10%, 20%, 30%, and 40% are as follows: 1194K, 1189K, 1186K, 1175K, and 1171K, respectively. Therefore, the increase in coal gangue blending ratio results in enhanced mainstream velocity, shortening the residence time of fuel in the precalciner. Coupled with the lower volatility and slower ignition of coal gangue, this leads to a reduction in the average outlet temperature as the blending ratio increases.

4.1.3 Influence on Raw Material Decomposition and Component Distribution

In Fig 6 when a lot of oxygen (O_2) is introduced at the tertiary air inlet, the CO_2 level in the area rises quickly. This is because burning pulverized coal uses up a lot of O_2 and gives off heat and CO_2. Apart from a gradual temperature decrease due to endothermic raw material decomposition, no conspicuous alterations occur in the trends of other component mass fractions. Injecting upper tertiary air slightly raises O_2, which, along with the ongoing burning of unburned materials and the breakdown of raw materials, causes the concentration of CO_2 to rise at first and then level off after the upper tertiary air dilutes it. With an increasing blending ratio, the non-combustible portion of coal gangue fuel imposes a certain restraint on combustion, reducing CO_2 concentration in combustion products. However, from the perspective of raw material decomposition, the overall airflow velocity enhancement accelerates the heat transfer process, allowing raw materials to rapidly absorb combustion reaction heat, and thus elevating CO_2 content. Nonetheless, in general, the CO_2 content at the outlet decreases with an increasing blending ratio.

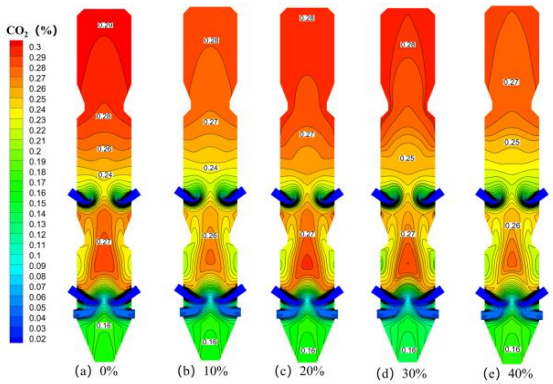

Fig. 6 The contour of CO_2 in different gangue mixing ratios

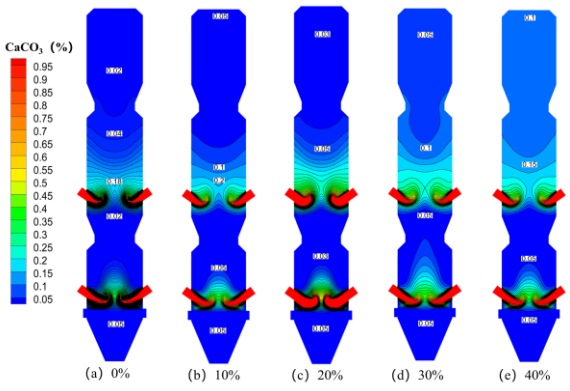

Fig. 7 The contour of $CaCO_3$ in different gangue mixing ratios

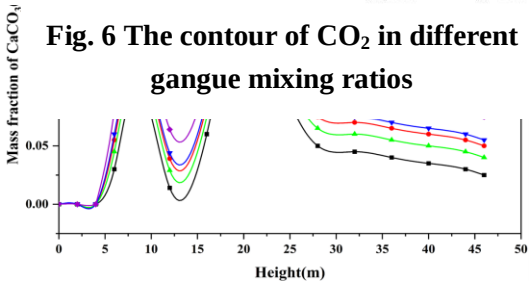

Fig. 8 Average $CaCO_3$ mass fraction in cross section at different gangue mixing ratios

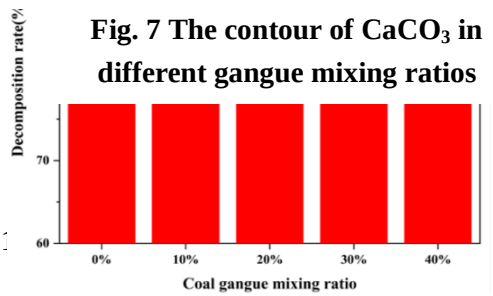

Fig. 9 Decomposition rate of raw material under different gangue mixing ratio

Fig 7 reveals that despite varying coal gangue content, the distribution of $CaCO_3$ mass fraction remains roughly consistent. In the vicinity of the upper and lower raw material inlets, the $CaCO_3$ mass fraction is high and diminishes rapidly upward. Additionally, under all five conditions, the decrease in $CaCO_3$ is more rapid in the lower column than in the upper column. Fig 8 depicts the average mass fraction of $CaCO_3$ along the height of the precalciner, demonstrating that the mass fraction of $CaCO_3$ at each working condition has two peaks at 8m and 20m of the decomposition furnace, which corresponds to the locations of the raw material inlet.. Fig 9 indicates that the raw material decomposition rates for coal gangue blending ratios of 0%, 10%, 20%, 30%, and 40% are 92.99%, 90.72%, 91.12%, 89.42%, and 87.43%, respectively. With an increase in the blending ratio, the raw material decomposition rate initially decreases, then increases, and subsequently continues to decrease as coal gangue content rises, consistent with the results shown in Fig 9. Therefore, a 20% coal gangue blend optimizes the raw material decomposition rate, establishing the basis for subsequent enriched oxygen combustion simulations with a 20% coal gangue blend.

4.2. Combustion Simulation of 20% Coal Gangue Blend under Various Oxygen-Enriched Atmospheres

4.2.1 Temperature Distribution Comparison

Fig 10 displays the temperature contour maps at the X=0 cross-section corresponding to different oxygen concentrations. It is discernible from the figure that as the oxygen concentration escalates, the high-temperature zone in the lower part of the precalciner progressively expands, while the peak temperature within the precalciner continuously rises. The main reason for this is that the higher oxygen concentration speeds up the combustion of the pulverized coal, making its combustion characteristics better. This advances the coal's burnout and ignition timings, which makes the coal reactions stronger. As a result, a significant temperature surge occurs in the primary coal combustion zones of the precalciner.

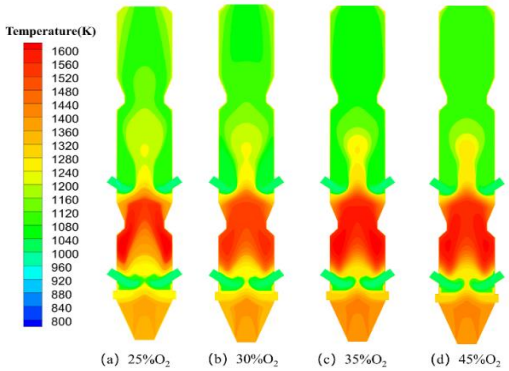

Fig.10 Temperature cloud diagram of X=0 section under different O_2 concentrations

Simultaneously, the temperature distribution within the precalciner is influenced by the raw material decomposition process. Under the combined effects of velocity and $CaCO_3$ decomposition, temperatures near the raw material inlet are comparatively lower. However, with an increase in oxygen content, temperatures from the raw material duct to the outlet position in the upper part of the precalciner gradually diminish. This reduction is mainly due to the elevated oxygen concentration fostering an increase in internal temperature, thereby accelerating $CaCO_3$ decomposition. Since $CaCO_3$ decomposition is an endothermic process, it leads to a gradual temperature decline in the upper column of the precalciner. The average outlet temperatures under the four conditions are as follows: 25% O_2 (1182K), 30% O_2 (1175K), 35% O_2 (1168K), and 40% O_2 (1161K). With an O_2 concentration of 40%, the outlet average temperature registers 1161K, reflecting a decrease of 21K compared to the scenario with a 25% O_2 concentration.

4.2.2 Impact on Raw Material Decomposition and Component Distribution

Fig 11 and Fig 12 present the distribution contour maps of $CaCO_3$ and CaO at the X=0 cross-section, corresponding to varying oxygen concentrations. As depicted in the figures, the

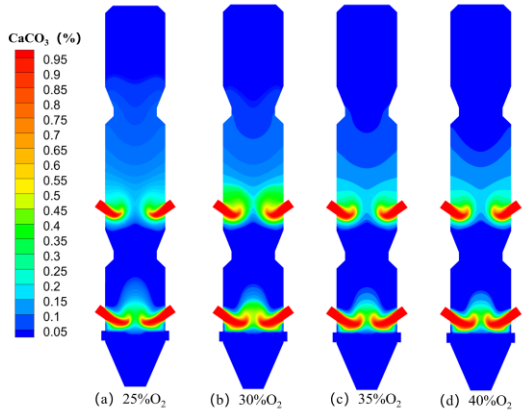

Fig. 11 Distribution cloud diagram of $CaCO_3$ at cross-section X=0 under different O_2 concentrations

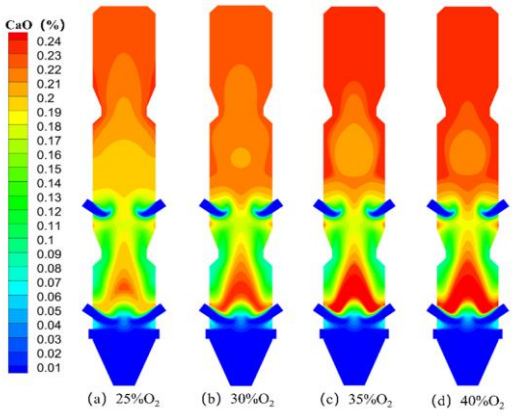

Fig. 12 Distribution cloud diagram of CaO at cross-section X=0 under different O_2 concentrations

concentration of $CaCO_3$ is predominantly localized near the upper and lower raw material ducts. When the O_2 concentration increases from 25% to 40%, there is a discernible decrease in the concentration of $CaCO_3$ near the precalciner's raw material duct, coupled with a corresponding increment in the CaO concentration. This pattern underscores that elevating the oxygen content effectively catalyzes the decomposition of $CaCO_3$. Moreover, the decomposition rate of $CaCO_3$ at the lower feed inlet notably surpasses that at the upper inlet, consistent with the temperature distribution profile.

A comparative analysis of Fig 11 and Fig 12 reveals that the fluctuations in $CaCO_3$ and CaO within the lower column of the precalciner are inconspicuous, indicating a marginal acceleration in the decomposition rate of the injected $CaCO_3$ in the precalciner's lower segment. This segment, being the primary combustion zone, experiences thermal saturation due to the heat generated from combustion, constraining further $CaCO_3$ decomposition. On the other hand, the significant variation in the $CaCO_3$ decomposition rate at the upper inlet is primarily due to the influence of temperature and CO_2 partial pressure on the decomposition process. The elevation in O_2 concentration enhances coal combustion, raising the temperature in the upper column of the precalciner and thereby promoting $CaCO_3$ decomposition therein. In summary, the increase in oxygen concentration elevates the average temperature and span of the high-temperature zones within the precalciner, thereby augmenting the $CaCO_3$ decomposition rate.

Table 5.Raw material compositions/wt%

Different O_2 concentrations	25%	30%	35%	40%
Raw material decomposition rate	92.6%	94.6%	95.2%	96.1%

Tab 5 delineates the correlation between the raw material decomposition rate and varying O_2 concentrations. It is evident from the table that the raw material decomposition rate escalates rapidly with increased O_2 concentration, achieving 96.1% when the O_2 proportion is 40%. This rate signifies a 3.5% enhancement compared to the conditions at a 25% O_2 concentration.

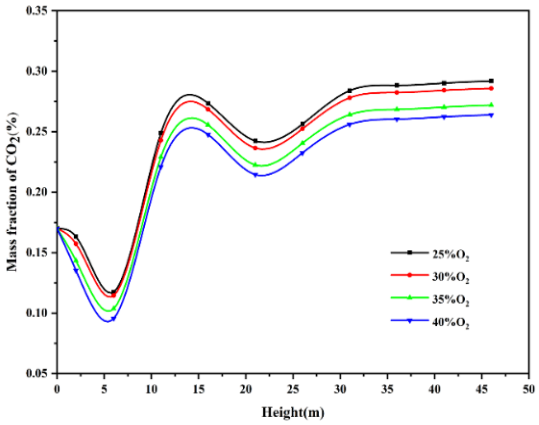

Fig. 13 Variation curves of CO_2 mass fraction at different O_2 concentrations

The concentration of CO_2 within the precalciner is primarily influenced by fuel combustion and raw material decomposition. As depicted in Fig 13, under conditions incorporating tertiary air and raw material addition, there is a discernible decrease in CO_2 concentration near the inlets of tertiary air and raw material within the precalciner. With an increase in O_2 concentration, the internal temperature of the precalciner rises, effectively promoting the decomposition of $CaCO_3$ and consequently elevating the concentration of CO_2 to a certain extent. However, the escalation in O_2 concentration intensifies the dilution effect of flue gas on CO_2 within the precalciner. Since the dilution by flue gas significantly outweighs the CO_2 generated from fuel combustion and material decomposition, there is a gradual decrement in the molar fraction of CO_2 within the precalciner as O_2 concentration increases. Concurrently, the enriched CO_2 at the precalciner outlet progressively declines, reaching 26.4% when the O_2 concentration is 40%, marking a 2.8% reduction compared to the scenario with 25% O_2.

5. Conclusions

(1) In simulating the combustion of various coal gangue blend ratios within the TTF precalciner, consistency was maintained in the inlet and outlet structures. The overall layout of the temperature field for mixed fuels and single fuels exhibited prominent symmetry on the X-section. Due to the distinct combustion characteristics of coal gangue and pulverized coal, including differing ignition temperatures and calorific values, the blending of coal gangue resulted in increased mainstream velocity, consequently shortening the fuel's residence time within the furnace. This effect led to a decrease in the average outlet temperature as the blending ratio increased.

With the help of the disturbance from the tertiary air, CO_2, a byproduct of fuel combustion and raw material decomposition, ascends parallel to the precalciner's central axis. Accordingly, the CO_2 concentration under various blending ratios increases with furnace height, with the CO_2 content at the outlet decreasing as the blending ratio rises. Post-processing of the average mass fraction of $CaCO_3$ at the outlet revealed raw material decomposition rates under 0%-40% coal gangue blending conditions as follows: 92.99%, 90.72%, 91.12%, 89.42%, and 87.43%. Taking into account the comprehensive decomposition rate, an optimal coal-gangue blending ratio is identified at 20%.

With an increasing blending proportion, the raw material decomposition rate initially decreases, then increases, and continues to decrease with further inclusion of coal gangue, reaching its peak at a 20% coal gangue blend.

(2) Considering the collective impact of varying oxygen-enriched atmospheres on precalciner temperature, components, and raw material decomposition, it was observed that at a 20% coal gangue combustion blend, enhancing the O_2 concentration could accelerate the fuel combustion rate and increase the temperature in localized high-temperature zones within the precalciner. The raw material decomposition rate swiftly rises with increasing O_2 concentration, achieving 96.1% at a 40% O_2 concentration ratio. This rate is a 3.5% improvement compared to the conditions at a 25% O_2 concentration.

Conflicts of Interest: The authors declare that they have no conflicts of interest to report regarding the present study.

References

[1] Hasanbeigi A, Price L, Lin E. Emerging energy-efficiency and CO2 emission-reduction technologies for cement and concrete production: A technical review[J]. Renewable and Sustainable Energy Reviews, 2012, 16(8): 6220-6238.

[2] Li J, Wang J. Comprehensive utilization and environmental risks of coal gangue: A review[J]. Journal of Cleaner Production, 2019, 239: 117946.

[3] Chuncai Z, Guijian L, Dun W, et al. Mobility behavior and environmental implications of trace elements associated with coal gangue: A case study at the Huainan Coalfield in China[J]. Chemosphere, 2014, 95: 193-199.

[4] Zhang Y, Nakano J, Liu L, et al. Co-combustion and emission characteristics of coal gangue and low-quality coal[J]. Journal of Thermal Analysis and Calorimetry, 2015, 120(3): 10.

[5] Zhang Y, Li J, Cheng F, et al. Study of the combustion behavior and kinetics of different types of coal gangue[J]. Combustion, Explosion, and Shock Waves, 2015, 51(6).

[6] Hanmin X, Xiaoqian M, Kai L. Co-combustion kinetics of sewage sludge with coal and coal gangue under different atmospheres[J]. Energy Conversion and Management, 2010, 51(10).

[7] Li B, Liu G, Gao W, et al. Study of combustion behaviour and kinetics modelling of Chinese Gongwusu coal gangue: Model-fitting and model-free approaches[J]. Fuel, 2020, 268: 117284.

[8] Chuncai Zou, Guijian Liu, Ting Fang, et al. Investigation on thermal and trace element characteristics during co-combustion biomass with coal gangue[J]. Bioresource Technology, 175 (2015), pp. 454-462.

[9] Fu Q, Huang Y, Niu M, et al. Experimental study on refuse derived fuel gasification with oxygen-rich air in fluidized bed gasifier[J]. Zhejiang Daxue Xuebao (Gongxue Ban)/Journal of Zhejiang University (Engineering Science), 2014, 48(7): 1265-1271.

[10] Zhang L, Wei X, Zhang Z, et al. Modeling De-NOx by Injection Ammonia in High Temperature Zone of Cement Precalciner[J]. Journal of Thermal Science, 2021, 30(2): 636-643.

[11] Fidaros D K, Baxevanou C A, Dritselis C D, et al. Numerical modelling of flow and transport processes in a calciner for cement production[J]. Powder Technology, 2006, 171(2).

[12] Wang W, Li F, Wang H. Numerical simulation study on the effect of different oxygen-enrichment atmospheres on diesel combustion[J]. Energy (Oxford), 2023, 266: 126474.

[13] Zhu J, Kao H. Numerical Simulation of Co-Combustion of Pulverized Coal and Different Proportionsof Refused Derived Fue lin TTF Precalciner[J]. Journal of Renewable Materials, 2021, 9(7): 15..

[14] Kangwanpongpan T, Corrêa Da Silva R, Krautz H J. Prediction of oxy-coal combustion through an optimized weighted sum of gray gases model[J]. Energy, 2012, 41(1): 244-251.

[15] Ariyaratne W K H, Malagalage A, Melaaen M C, et al. CFD modelling of meat and bone meal combustion in a cement rotary kiln – Investigation of fuel particle size and fuel feeding position impacts[J]. Chemical Engineering Science, 2015, 123: 596-608.

[16] Rahmanian B, Safaei M R, Kazi S N, et al. Investigation of pollutant reduction by simulation of turbulent non-premixed pulverized coal combustion[J]. Applied Thermal Engineering, 2014, 73(1): 1222-1235.

[17] Gómez M A, Porteiro J, de la Cuesta D, et al. Numerical simulation of the combustion process of a pellet-drop-feed boiler[J]. Fuel, 2016, 184: 987-999.

[18] Branco J, Coelho P J, Costa M. Experimental and numerical investigation of turbulent diffusion flames in a laboratory combustor with a slot burner[J]. Fuel, 2016, 175: 182-190.

[19] Mikulčić H, von Berg E, Vujanović M, et al. Numerical analysis of cement calciner fuel efficiency and pollutant emissions[J]. Clean Technologies and Environmental Policy, 2013, 15(3): 489-499.

[20] Kobayashi H, Howard J B, Sarofim A F. Coal devolatilization at high temperatures[J]. Symposium (International) On Combustion, 1977, 16(1): 411-425.

[21] Amila Chandra Kahawalage Morten C. Melaaen Lars-André Tokheim, Numerical modelling of the calcination process in a cement kiln system 2017. Proceedings of the 58th SIMS
September 25th - 27th, Reykjavik, Iceland

Submitted: 30.11.2023.
Revised: 28.01.2024.
Accepted: 01.02.2024.